Bounds on the difference between reconstructions in binary tomography

K. Joost Batenburg[1,2], Wagner Fortes[1,3], Lajos Hajdu[4,5], and Robert Tijdeman[3]

[1] Centrum Wiskunde & Informatica, Amsterdam, The Netherlands,
joost.batenburg@cwi.nl
[2] Vision Lab, University of Antwerp, Belgium
[3] Mathematical Institute, Leiden University, The Netherlands
[4] Institute of Mathematics, University of Debrecen, Hungary
[5] Number Theory Research Group of the Hungarian Academy of Sciences, Debrecen, Hungary

Abstract. Tomography is concerned with the reconstruction of images from their projections. In this paper, we consider the reconstruction problem for a class of tomography problems, where the images are restricted to binary grey levels. For any given set of projections, we derive an upper bound on the difference between any two binary images having these projections, and a bound on the difference between a *particular* binary image and any binary image having the given projections. Both bounds are evaluated experimentally for different geometrical settings, based on simulated projection data for a range of images.

1 Introduction

The field of *tomography* studies the problem of reconstructing an object from its projections, recorded along a range of viewing angles. Projection images are typically acquired by sending a certain beam (i.e., X-rays, electrons, neutrons) through the object, while measuring the attenuated beam profile that results after beam-object interaction. If a sufficient number of high-quality projection images are available, an accurate reconstruction of the object can be computed using a tomographic reconstruction algorithm [1, 2].

In various applications of tomography, only few projections can be acquired, or the range of available projection directions is limited. Such reconstruction problems are known as *limited-data problems*. In electron tomography, for example, the shape of the sample holder limits the angular range of the projections [3]. In industrial tomography for quality assurance, limitations on the duration of a scan impose an upper bound on the number of projections.

Applying classical reconstruction algorithms such as Filtered Backprojection to limited-data problems often results in inferior reconstruction quality. Several approaches have been proposed for overcoming these problems, by incorporating various forms of *prior knowledge* about the object in the reconstruction algorithm. The field of *discrete tomography* focuses on the reconstruction of images that consist of a small, discrete set of grey values [4, 5]. By exploiting the knowledge of these grey values in the reconstruction algorithm, it is often possible to compute accurate reconstructions from far fewer projections than required by classical "continuous" tomography algorithms. Still,

despite the discrete grey level assumption, the reconstruction problem may be underdetermined and a large number of solutions may exist. In such cases, it can be important to know how different these solutions can be. If one can give a bound on the maximum difference between two solutions, this also bounds the maximum difference between the unknown ground truth image, of which projections have been measured, and any other solution.

In this paper, we focus on *binary* reconstruction problems, where the unknown image is known to have only two grey levels, 0 and 1. The problem of bounding the difference between binary reconstructions is closely related to the *stability problem*, which concerns the question how the reconstruction changes if the projections are slightly modified [6–9]. In [10, 11], Van Dalen presented sharp bounds on the difference between any two binary images having the *same* projections for the case of two projections: horizontal and vertical.

The bound we present here is much more general, as it can incorporate an arbitrary number of projections and can even be applied in different geometrical settings (lattice images, as well as discretized continuous images). It is based on the observation first made by Hajdu and Tijdeman in [12], that the Euclidean norm of all binary solutions does not depend on the particular solution, and can be determined directly from the projections. Using a multi-dimensional variant of Pythagoras' theorem, this allows for bounding the Euclidean norm of the difference between two such solutions. Although the resulting bound will not be strict in general, it is the first general bound for binary tomography problems that can be used in a wide range of reconstruction problems.

This paper is structured as follows. In Section 2, we define a general class of reconstruction problems and discuss two specific examples of such problems, for lattice images and a strip projection model, respectively. We also introduce notation and recall some basic properties. In Section 3, a general bound is derived on the difference between two binary images having a given set of projections. In Section 4, a bound is derived on the difference between a particular binary image, which is relatively easy to compute, and any binary solution of the tomography problem. Section 5 presents a series of simulation experiments and their results. From these results, the practical value of the proposed bounds can be evaluated for different types of images. Section 6 concludes the paper.

2 Notation and model

2.1 Tomography models

Throughout the discrete tomography literature, several imaging models have been considered. In the *grid model*, an image is formed by assigning a value to each point in a regular grid. In the case of binary images, each point is assigned a value of either 0 or 1. Here, we consider square grids of the form $A = \{(i, j) \in \mathbb{Z}^2 : 1 \leq i, j \leq s\}$ for $s \geq 1$; see Fig. 1(a). A *projection* is formed by considering the set of parallel lines through one or more grid points in a certain direction $(a, b) \in \mathbb{Z}^2$, with $a \geq 0$ and (a, b) coprime, and summing the values of the points on each line. The grid model can be used to model nanocrystals, that consist of discrete atoms positioned in a regular grid [13].

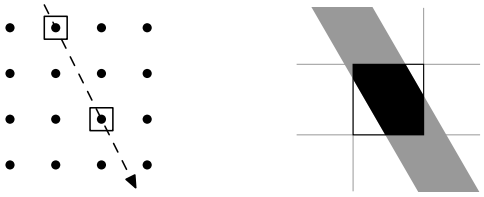

(a) Grid model (b) Strip model

Fig. 1. Two different projection models.

In many tomography applications, a *continuous* representation of the object is more realistic, as there is no intrinsic grid structure. In such cases, the unknown image is typically approximated by an image defined on a discrete pixel grid. A common model for computing the projections of such a pixelized image is the *strip model*. In the strip model, a projection is computed by considering a set of parallel strips in a given direction and computing a weighted sum of all the pixels that intersect with each strip, with a weight that is determined by the intersection area between the strip and the pixel.

We now define some general notation. An *image* is represented by a vector $\boldsymbol{x} = (x_i) \in \mathbb{R}^n$. We refer to the entries of $\boldsymbol{x}$ as *pixels*, although they can also correspond with grid points, in the grid model. The derivation of our main results does not depend on the particular projection model. Throughout this paper we assume that all images are square, consisting of c rows and c columns, where $n = c^2$. A *binary image* corresponds with a vector $\bar{\boldsymbol{x}} \in \{0, 1\}^n$.

For a given set of k projection directions, the *projection map* maps an image $\boldsymbol{x}$ to a vector $\boldsymbol{p} \in \mathbb{R}^m$ of *projection data*, where m denotes the total number of line measurements. As the projection map is a linear transformation, it can be represented by a matrix $\boldsymbol{W} = (w_{ij}) \in \mathbb{R}^{m \times n}$, called the *projection matrix*. Entry w_{ij} represents the weight of the contribution of x_j to projected line i. Note that for the grid model the projection matrix is a binary matrix, while for the strip model its entries are real values in $[0, 1]$. The projection matrix $\boldsymbol{W}$ and vector $\boldsymbol{p}$ can be decomposed into k blocks as

$$\boldsymbol{W} = \begin{pmatrix} \boldsymbol{W}^1 \\ \vdots \\ \boldsymbol{W}^k \end{pmatrix}, \quad \boldsymbol{p} = \begin{pmatrix} \boldsymbol{p}^1 \\ \vdots \\ \boldsymbol{p}^k \end{pmatrix}, \tag{1}$$

where each block $\boldsymbol{W}^d$ $(d = 1, \ldots, k)$ represents the projection map for a single direction and each block $\boldsymbol{p}^d$ represents the corresponding projection data.

From this point on, we assume that the projection matrix has the property that $\sum_{i=1}^{m} w_{ij} = k$ for all $j = 1, \ldots, n$. This property is certainly satisfied for the grid model, as every x_j is counted with weight 1 for exactly one line in each projection direction. The property is also satisfied for the strip projection model, as the total pixel weight for each projection angle is equal to the area of a pixel, which is 1. Note that the property is *not* satisfied for some other models commonly used in tomography, such as the line

model, where the weight of a pixel is determined by the length of its intersection with a line.

The *general reconstruction problem* consists of finding a solution of the system $\boldsymbol{Wx} = \boldsymbol{p}$ for given projection data $\boldsymbol{p}$, i.e., to find an image that has the given projections. In *binary tomography*, one seeks a binary solution of the system. For a given projection matrix $\boldsymbol{W}$ and given projection data $\boldsymbol{p}$, let $S_{\boldsymbol{W}}(\boldsymbol{p}) := \{\boldsymbol{x} \in \mathbb{R}^n : \boldsymbol{Wx} = \boldsymbol{p}\}$, the set of all real-valued solutions corresponding with the projection data, and let $\bar{S}_{\boldsymbol{W}}(\boldsymbol{p}) := S_{\boldsymbol{W}}(\boldsymbol{p}) \cap \{0,1\}^n$, the set of *binary solutions* of the system. As the main goal of incorporating prior knowledge of the binary grey levels in the reconstruction is to reduce the number of required projections, we focus on the case where m is small with respect to n, such that the real-valued reconstruction problem is severely underdetermined.

As the projection matrix is typically not a square matrix, and also does not have full rank, it does not have an inverse. Recall that the *Moore-Penrose pseudo inverse* of an $m \times n$ matrix $\boldsymbol{A}$ is an $n \times m$ matrix $\boldsymbol{A}^\dagger$, satisfying the following four conditions

1. $\boldsymbol{A}\boldsymbol{A}^\dagger\boldsymbol{A} = \boldsymbol{A}^\dagger$;
2. $\boldsymbol{A}^\dagger\boldsymbol{A}\boldsymbol{A}^\dagger = \boldsymbol{A}$;
3. $(\boldsymbol{A}\boldsymbol{A}^\dagger)^T = \boldsymbol{A}\boldsymbol{A}^\dagger$;
4. $(\boldsymbol{A}^\dagger\boldsymbol{A})^T = \boldsymbol{A}^\dagger\boldsymbol{A}$.

For any matrix $\boldsymbol{A}$, there exists such a matrix $\boldsymbol{A}^\dagger$, which is unique; see [14].

Let $\boldsymbol{x}^* = \boldsymbol{W}^\dagger\boldsymbol{p}$. Then $\boldsymbol{x}^*$ has the following properties (see Chapter 3 of [14]): (i) it is the solution of the system $\boldsymbol{Wx} = \boldsymbol{p}$ of minimal Euclidean norm. (ii) it is orthogonal to the nullspace $\mathcal{N}(\boldsymbol{W})$ of $\boldsymbol{W}$. We call $\boldsymbol{x}^*$ the *central reconstruction* of $\boldsymbol{p}$. The central reconstruction plays an important role in the binary reconstruction problem. We will show in the next section that all binary solutions of the system have equal distance to $\boldsymbol{x}^*$, so that one can consider the central reconstruction as lying "in the middle" of all binary solutions.

As our bounds on the distance between binary solutions depend on $\boldsymbol{x}^*$, computation of $\boldsymbol{x}^*$ is necessary to compute the corresponding distance bounds. Due to the size of the matrix $\boldsymbol{W}$, explicit calculation of $\boldsymbol{W}^\dagger$ is usually unpractical for large images. As an alternative, an iterative method for solving the system $\boldsymbol{Wx} = \boldsymbol{p}$, called *CGLS* (Conjugate Gradient Least Squares), can be used [15]. Apart from numerical errors, applying CGLS to the system $\boldsymbol{Wx} = \boldsymbol{p}$ results, after convergence, in the computation of $\boldsymbol{W}^\dagger\boldsymbol{p}$, while not computing the matrix $\boldsymbol{W}^\dagger$ explicitly (see also [16]).

3 A bound on the difference between all binary solutions

We start this section by showing that the Euclidean norm of any binary solution of $\boldsymbol{Wx} = \boldsymbol{p}$ is completely determined by $\boldsymbol{p}$.

Lemma 1. *Let $\bar{\boldsymbol{x}} \in \bar{S}_{\boldsymbol{W}}(\boldsymbol{p})$. Then, $\|\bar{\boldsymbol{x}}\|_2^2 = \frac{\|\boldsymbol{p}\|_1}{k}$.*

Proof. By the definition of the ℓ_1-norm, $\|\boldsymbol{p}\|_1 = \sum_{i=1}^m |p_i| = \sum_{i=1}^m p_i$, since $p_i \geq 0$ ($i = 1, \ldots, n$). Also,

$$\sum_{i=1}^{m} p_i = \sum_{i=1}^{m} \left(\sum_{j=1}^{n} w_{ij} \bar{x}_j \right) = \sum_{j=1}^{n} \left(\sum_{i=1}^{m} w_{ij} \right) \bar{x}_j = \sum_{j=1}^{n} k \bar{x}_j, \tag{2}$$

and therefore $\|\boldsymbol{p}\|_1 = k \sum_{j=1}^{n} \bar{x}_j$.

As $\bar{\boldsymbol{x}} \in \{0,1\}^n$, we have $\|\bar{\boldsymbol{x}}\|_2^2 = \|\bar{\boldsymbol{x}}\|_1 = \sum_{j=1}^{n} \bar{x}_j = \frac{\|\boldsymbol{p}\|_1}{k}$.

□

The following lemma illustrates the importance of the central reconstruction, the shortest real-valued solution in $S_{\boldsymbol{W}}(\boldsymbol{p})$, by showing that the binary solutions are the shortest among all integer solutions of the system.

Lemma 2. *Let $\bar{\boldsymbol{x}} \in \bar{S}_{\boldsymbol{W}}(\boldsymbol{p})$ and $\boldsymbol{y} \in S_{\boldsymbol{W}}(\boldsymbol{p}) \cap \mathbb{Z}^n$. Then $\|\bar{\boldsymbol{x}}\|_2 \leq \|\boldsymbol{y}\|_2$, with equality if and only if $\boldsymbol{y} \in \bar{S}_{\boldsymbol{W}}(\boldsymbol{p})$.*

Proof. Note that the statement is proved in [12], see Problem 2 and the subsequent paragraph. However, for the convenience of the reader we give the proof here.

We have

$$\|\bar{\boldsymbol{x}}\|_2^2 = \sum_{i=1}^{n} \bar{x}_i^2 = \sum_{i=1}^{n} \bar{x}_i = \sum_{i=1}^{n} y_i = \frac{\sum_{j=1}^{m} p_j}{k}. \tag{3}$$

Observing that

$$\sum_{i=1}^{n} y_i \leq \sum_{i=1}^{n} y_i^2 = \|\boldsymbol{y}\|_2^2, \tag{4}$$

with equality if and only if $\boldsymbol{y}$ is binary, yields the result. □

Supposing the existence of at least two different binary solutions, Lemma 1 allows us to derive an upper bound for the Euclidean distance between those solutions.

Theorem 1. *Let $\bar{\boldsymbol{x}}, \bar{\boldsymbol{y}} \in \bar{S}_{\boldsymbol{W}}(\boldsymbol{p})$ and $\boldsymbol{x}^* = \boldsymbol{W}^\dagger \boldsymbol{p}$. Then, $\|\bar{\boldsymbol{y}} - \bar{\boldsymbol{x}}\|_2 \leq 2R$, where $R := \sqrt{\frac{\|\boldsymbol{p}\|_1}{k} - \|\boldsymbol{x}^*\|_2^2}$.*

Proof. From the definition of $\boldsymbol{x}^*$ we have $(\bar{\boldsymbol{x}} - \boldsymbol{x}^*) \in \mathcal{N}(\boldsymbol{W})$, and $\boldsymbol{x}^* \perp (\bar{\boldsymbol{x}} - \boldsymbol{x}^*)$. Using Pythagoras' theorem and Lemma 1 yields

$$\|\bar{\boldsymbol{x}} - \boldsymbol{x}^*\|_2^2 = \frac{\|\boldsymbol{p}\|_1}{k} - \|\boldsymbol{x}^*\|_2^2 = R^2, \tag{5}$$

which means that any binary solution is on the hypersphere centered in $\boldsymbol{x}^*$ with radius $\sqrt{\frac{\|\boldsymbol{p}\|_1}{k} - \|\boldsymbol{x}^*\|_2^2}$. Therefore,

$$\|\bar{\boldsymbol{x}} - \bar{\boldsymbol{y}}\|_2 \leq \|\bar{\boldsymbol{x}} - \boldsymbol{x}^*\|_2 + \|\bar{\boldsymbol{y}} - \boldsymbol{x}^*\|_2 = 2R.$$

□

Corollary 1. *Let $\bar{\boldsymbol{x}}, \bar{\boldsymbol{y}} \in \bar{S}_{\boldsymbol{W}}(\boldsymbol{p})$. Then $\|\bar{\boldsymbol{x}} - \bar{\boldsymbol{y}}\|_1 \leq 4(\frac{\|\boldsymbol{p}\|_1}{k} - \|\boldsymbol{x}^*\|_2^2)$.*

Proof. As $\bar{\boldsymbol{x}}$ and $\bar{\boldsymbol{y}}$ are binary, we have $\|\bar{\boldsymbol{x}} - \bar{\boldsymbol{y}}\|_1 = \|\bar{\boldsymbol{x}} - \bar{\boldsymbol{y}}\|_2^2$. The corollary now follows directly from Theorem 1. □

The norm $\|\bar{\boldsymbol{x}} - \bar{\boldsymbol{y}}\|_1$ corresponds to the number of pixels that are different between $\bar{\boldsymbol{x}}$ and $\bar{\boldsymbol{y}}$. As one is typically mainly interested in the *fraction* of pixels that can be different, we introduce the *variability* of $(\boldsymbol{W}, \boldsymbol{p})$, defined by $V := \frac{4R^2}{n}$, which is an upper bound for the fraction of pixels that are different between any two binary solutions.

4 A bound on the difference with a particular binary image

The fact that all elements of $\bar{S}_{\boldsymbol{W}}(\boldsymbol{p})$ have equal distance to the central reconstruction $\boldsymbol{x}^*$, combined with the facts that binary solutions are the shortest solutions among all integer solutions (Lemma 2) and that $\boldsymbol{x}^*$ is the shortest real-valued solution, suggests that binary solutions can often be found near $\boldsymbol{x}^*$. It is therefore natural to consider the image that is obtained by rounding each entry of $\boldsymbol{x}^*$ to the nearest binary value.

Let $\langle\alpha\rangle = \min(|\alpha|, |\alpha - 1|)$ for $\alpha \in \mathbb{R}$, and put $T = \sqrt{\sum_{i=1}^{n} \langle x_i^* \rangle^2}$, i.e., the Euclidean distance from $\boldsymbol{x}^*$ to the nearest binary vector.

Corollary 2. *If $R < T$, then $\bar{S}_{\boldsymbol{W}}(\boldsymbol{p}) = \emptyset$.*

If $R = T$, then all solutions in $\bar{S}_{\boldsymbol{W}}(\boldsymbol{p})$ can be obtained by rounding the values in $\boldsymbol{x}^*$ to the nearest binary values, and variations are only possible for the entries i where $x_i^* = \frac{1}{2}$.

Let $\bar{\boldsymbol{r}} \in \{0, 1\}^n$ such that $\|\bar{\boldsymbol{r}} - \boldsymbol{x}^*\|_2 = T$, i.e., $\bar{\boldsymbol{r}}$ is among the binary vectors that are nearest to $\boldsymbol{x}^*$ in the Euclidean sense. If $R > T$ and $R - T$ is small, it is possible to say that a fraction of the rounded values are correct, i.e., to provide an upper bound on the *number* of pixel differences between any solution in $\bar{S}_{\boldsymbol{W}}(\boldsymbol{p})$ and $\bar{\boldsymbol{r}}$.

In most cases we can not say *which* rounded values are correct. Suppose that $\bar{\boldsymbol{x}} \in \bar{S}_{\boldsymbol{W}}(\boldsymbol{p})$ and that $\bar{r}_i = 1$ whereas $\bar{x}_i = 0$. Note that we have $x_i^* \geq \frac{1}{2}$. Put $\tilde{\boldsymbol{r}} := \bar{\boldsymbol{r}}$ and then set $\tilde{r}_i$ to 0. We then have $\|\tilde{\boldsymbol{r}} - \boldsymbol{x}^*\|_2^2 = \|\bar{\boldsymbol{r}} - \boldsymbol{x}^*\|_2^2 - |x_i^* - 1|^2 + |x_i^*|^2 = \|\bar{\boldsymbol{r}} - \boldsymbol{x}^*\|_2^2 + 2x_i^* - 1$. Similarly, if $\bar{r}_i = 0$, then the squared Euclidean distance increases by $1 - 2x_i^*$ by setting pixel i to 1. Each time an entry i of $\bar{\boldsymbol{r}}$ is changed, the squared Euclidean distance to $\boldsymbol{x}^*$ increases by $b_i := |2x_i^* - 1|$.

As the Euclidean distance from $\boldsymbol{x}^*$ to $\bar{\boldsymbol{x}}$ is R, a bound can now be derived on the maximal number of pixels in $\bar{\boldsymbol{r}}$ that must be changed to move from $\bar{\boldsymbol{r}}$ to $\bar{\boldsymbol{x}}$.

Let us order the values b_i $(i = 1, \ldots, n)$ such that $b_i \leq b_{i+1}$ for $1 \leq i \leq n - 1$. Assuming that $\bar{S}_{\boldsymbol{W}}(\boldsymbol{p}) \neq \emptyset$, we have $R \geq \|\bar{\boldsymbol{r}} - \boldsymbol{x}^*\|_2$ and the change of s entries of $\bar{\boldsymbol{r}}$ would increase the distance between $\bar{\boldsymbol{r}}$ and $\boldsymbol{x}^*$ such that $R^2 \geq \|\bar{\boldsymbol{r}} - \boldsymbol{x}^*\|_2^2 + \sum_{j=1}^{s} b_j$.

Theorem 2. *Let $\bar{\boldsymbol{r}}$, $\bar{\boldsymbol{x}}$ and b_i $(i = 1, \ldots, n)$ be as defined above. Choose s such that*

$$\sum_{i=1}^{s} b_i \leq R^2 - \|\bar{\boldsymbol{r}} - \boldsymbol{x}^*\|_2^2 < \sum_{j=1}^{s+1} b_j. \tag{6}$$

Then at most s pixels can have the wrong value in $\bar{\boldsymbol{r}}$ with respect to $\bar{\boldsymbol{x}}$ and at least $n - s$ pixels must have the correct value.

Proof. Due to the increasing order of the b_i's, changing more than s pixels in $\bar{\boldsymbol{r}}$ will result in a vector $\tilde{\boldsymbol{r}}$ for which $\|\tilde{\boldsymbol{r}} - \boldsymbol{x}^*\|_2 > R$, which cannot be an element of $\bar{S}_{\boldsymbol{W}}(\boldsymbol{p})$. □

Corollary 3. *Let $\bar{\boldsymbol{r}}$ and s be as in Theorem 2. Let $\bar{\boldsymbol{x}}, \bar{\boldsymbol{y}} \in \bar{S}_{\boldsymbol{W}}(\boldsymbol{p})$. Then $\|\bar{\boldsymbol{x}} - \bar{\boldsymbol{y}}\|_1 \leq 2s$.*

In fact, Corollary 3 can be sharpened as follows. Theorem 2 bounds the number of pixel differences between $\bar{\boldsymbol{x}}$ and $\bar{\boldsymbol{r}}$, and between $\bar{\boldsymbol{y}}$ and $\bar{\boldsymbol{r}}$. When using these two bounds to determine an upper bound on the number of differences between $\bar{\boldsymbol{x}}$ and $\bar{\boldsymbol{y}}$, we can assume that these two sets of pixel differences are disjoint, as otherwise the difference between $\bar{\boldsymbol{x}}$ and $\bar{\boldsymbol{y}}$ will only be smaller. This observation leads to the following corollary:

Corollary 4. *Let $\bar{\boldsymbol{r}}$ and b_i $(i = 1, \ldots, n)$ be as defined above. Let $\bar{\boldsymbol{x}}, \bar{\boldsymbol{y}} \in \bar{S}_W(\boldsymbol{p})$. Choose t such that*

$$\sum_{i=1}^{t} b_i \leq 2(R^2 - \|\bar{\boldsymbol{r}} - \boldsymbol{x}^*\|_2^2) < \sum_{j=1}^{t+1} b_j. \tag{7}$$

Then at most t pixels can be different between $\bar{\boldsymbol{x}}$ and $\bar{\boldsymbol{y}}$.

5 Experiments and results

A series of experiments was performed to investigate the practical value of the bounds given in Theorems 1 and 2, for a range of images. The experiments are all based on simulated projection data obtained by computing the projections of the test images (so-called *phantoms*) in Fig. 2: (1) a simple, nearly convex object; (2) a more complex object, containing a small hole; (3) a cross-section of a cylinder head from a combustion engine; (4) a cross-section of femur rat bone. All phantoms have a size of 512×512 pixels. To perform images with varying image size (smaller than 512×512), the phantoms have been downscaled to obtain binary images of the appropriate sizes.

In each experiment, the central projection $\boldsymbol{x}^*$ was first computed using the CGLS algorithm. Based on the central reconstruction, the variability V was computed, and $\bar{\boldsymbol{r}}$ was computed by rounding $\boldsymbol{x}^*$ to the nearest binary vectors (choosing $\bar{r}_i = 1$ if $x_i^* = \frac{1}{2}$). The upper bound s from Theorem 2 on the number of differences between $\bar{\boldsymbol{r}}$ and the phantom image $\bar{\boldsymbol{x}}$ was then computed, followed by a bound on the fraction of pixel differences $U := \frac{s}{n}$, and the actual fraction of differences $E := \frac{e}{n}$, where e is the number of pixel differences between $\bar{\boldsymbol{r}}$ and $\bar{\boldsymbol{x}}$.

In the next subsections, the experimental results will be presented for the grid model and the strip model, respectively.

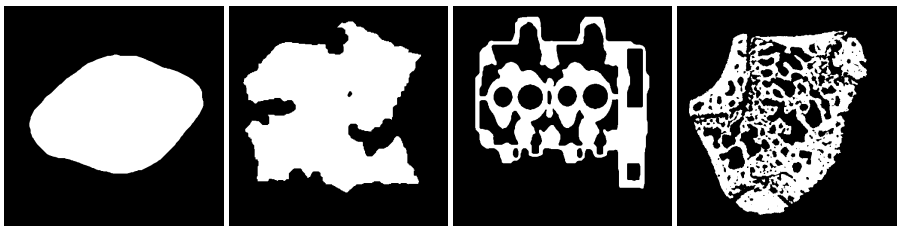

(a) Phantom 1 (b) Phantom 2 (c) Phantom 3 (d) Phantom 4

Fig. 2. Original phantom images used for the experiments.

In the grid model, a projection direction is represented by a pair of integers $(a, b) \in \mathbb{Z}^2$, such that $\gcd(a, b) = 1$ and $a \geq 0$. Let $\mathcal{A}$ be the set of all such pairs. For any positive integer c, put $\mathcal{A}_c := \{(a, b) \in \mathcal{A} : \max(a, |b|) = c\}$ and order the elements of $\mathcal{A}_c$, firstly by increasing value of a, secondly by increasing value of $|b|$, and thirdly by decreasing value of b. For example, $\mathcal{A}_3 = \{(1, 3), (1, -3), (2, 3), (2, -3), (3, 1), (3, -1), (3, 2), (3, -2)\}$. For any positive integer c, the ordered set $\mathcal{D}_c$ is formed by concatenating $\mathcal{A}_1, \ldots, \mathcal{A}_c$; for example, $\mathcal{D}_3 = \{(0, 1), (1, 0), (1, 1), (1, -1), (1, 2), (1, -2), (2, 1), (2, -1), (1, 3), (1, -3), (2, 3), (2, -3), (3, 1), (3, -1), (3, 2), (3, -2)\}$. To perform an experiment with k projection

angles, the first k directions were selected from the set $\mathcal{D}_{20}$. This means that when the number of direction is increased, the old set of directions is always included in the new set of directions.

Experiments have been performed based on the three phantom images, scaled to sizes of 32×32, 128×128 and 512×512 respectively, varying the number of projection directions. The results are shown in Fig. 3. In a second series of experiments, the size of the image was varied from 32×32 up to 512×512. When increasing the image width c, the number of pixels grows quadratically with c, while the number of line sums per projection direction grows linearly with c. To compare results for different image sizes, the ratio $\frac{c}{k}$, between the image width and the number of projection directions is kept constant, increasing the number of projection directions along with the image size. The ratio $\frac{c}{k}$ is chosen separately for each phantom, such that it leads to values near $U = 0.01$ for sufficiently large images.

The experiments for the strip model have been performed using projection angles equally distributed between 0 and 180 degrees. Projections have been computed based on sets of parallel strips, each strip having a width that equals the pixel size.

Experiments have been performed based on the three phantom images, scaled to sizes of 32×32, 128×128 and 512×512 respectively, varying the number of projection directions. The results are shown in Fig. 3. In a second series of experiments, the size of the image was varied from 32×32 up to 512×512. while keeping the ratio $\frac{c}{k}$ constant, increasing the number of projection directions along with the image size. The ratio $\frac{c}{k}$ is chosen separately for each phantom, such that it leads to values near $U = 0.01$ for sufficiently large images.

Despite the facts that the four phantoms have strong differences in shape and morphology, and that the grid and strip models are quite different, the results shown in Figs. 3-6 are surprisingly consistent throughout all experiments. Clearly, both the variability V and the upper bound U on the fraction of pixel differences between $\bar{\boldsymbol{r}}$ and $\boldsymbol{x}^*$ become smaller as the number of projection directions is increased. We see that the phantom $\bar{\boldsymbol{x}}$ is typically much closer to $\bar{\boldsymbol{r}}$ than to $\boldsymbol{x}^*$, and that the actual number of differences between these two images is approximated quite sharply by the upper bound U.

Fig. 5(c) and (d), part of the graphs for U and E are missing. In fact, in these cases both U and E are zero, such that they cannot be displayed in the logarithmic scale. This illustrates that Theorem 2 can be used to prove uniqueness of a binary solution, even when the corresponding real-valued system of equations is underdetermined.

In the strip model, the total number of measured line sums is given by ck, whereas the total number of unknown pixels is c^2. Fig. 6 illustrates that even if $\frac{c}{k} \geq 4$, the bound from Theorem 2 leads to a guarantee that the fraction of pixel differences between $\bar{\boldsymbol{x}}$ and $\bar{\boldsymbol{r}}$ is of the order of 1%, so $\bar{\boldsymbol{r}}$ is a very good approximation of the original binary image.

6 Outlook and conclusions

In this article, we have presented two general bounds on the accuracy of reconstructions in binary tomography, with respect to the unknown original object. The bounds can be computed efficiently and give guarantees on the number of pixels that can be

different between any two binary reconstructions that satisfy given line sums, and on the difference between a particular binary image, obtained by rounding the central projection to the nearest binary vector, and any binary image satisfying the projections. The experimental results show that by using these bounds, one can prove that the number of differences between binary reconstructions must be very small, even when the corresponding real-valued system of equations is severely underdetermined. In order to make these bound practically useful, our results will have to be extended to deal with noisy projection data, which we will incorporate in future research.

Acknowledgements

L.H. was supported by the OTKA grants K67580 and K75566, and by the TÁMOP 4.2.1./B-09/1/KONV-2010-0007 project. The project is implemented through the New Hungary Development Plan, cofinanced by the European Social Fund and the European Regional Development Fund. W.F. acknowledges support from the Erasmus Mundus program of the European Union.

References

1. Kak, A.C., Slaney, M.: Principles of Computerized Tomographic Imaging. SIAM (2001)
2. Herman, G.T.: Fundamentals of Computerized Tomography: Image reconstruction from projections. Springer (2009)
3. Midgley, P.A., Dunin-Borkowski, R.E.: Electron tomography and holography in materials science. Nature Materials **8**(4) (2009) 271–280
4. Herman, G.T., Kuba, A., eds.: Discrete Tomography: Foundations, Algorithms and Applications. Birkhäuser, Boston (1999)
5. Herman, G.T., Kuba, A., eds.: Advances in Discrete Tomography and its Applications. Birkhäuser, Boston (2007)
6. Alpers, A.: Instability and Stability in Discrete Tomography. PhD thesis, Technische Universität München (2003) Shaker Verlag, ISBN 3-8322-2355-X.
7. Alpers, A., Gritzmann, P.: On stability, error correction, and noise compensation in discrete tomography. SIAM Journal on Discrete Mathematics **20**(1) (2006) 227–239
8. Alpers, A., Brunetti, S.: Stability results for the reconstruction of binary pictures from two projections. Image and Vision Computing **25**(10) (2007) 1599–1608
9. Van Dalen, B.: Stability results for uniquely determined sets from two directions in discrete tomography. Discrete Mathematics **309** (2009) 3905–3916
10. Van Dalen, B.: On the difference between solutions of discrete tomography problems. Journal of Combinatorics and Number Theory **1** (2009) 15–29
11. Van Dalen, B.: On the difference between solutions of discrete tomography problems II. Pure Mathematics and Applications **20** (2009) 103–112
12. Hajdu, L., Tijdeman, R.: Algebraic aspects of discrete tomography. J. Reine Angew. Math. **534** (2001) 119–128
13. Jinschek, J.R., Batenburg, K.J., Calderon, H.A., Kilaas, R., Radmilovic, V., Kisielowski, C.: 3-d reconstruction of the atomic positions in a simulated gold nanocrystal based on discrete tomography: Prospects of atomic resolution electron tomography. Ultramicroscopy **108(6)** (2007) 589–604

14. Ben-israel, A., Greville, T.N.E.: Generalized inverses: Theory and applications. Canadian Math. Soc. (2002)
15. Saad, Y.: Iterative Methods for Sparse Linear Systems. SIAM, Philadelphia, PA, USA (2003)
16. Van der Sluis, A., Van der Vorst, H.A.: SIRT and CG-type methods for the iterative solution of sparse linear least-squares problems. Linear Algebra Appl. **130** (1990) 257–302

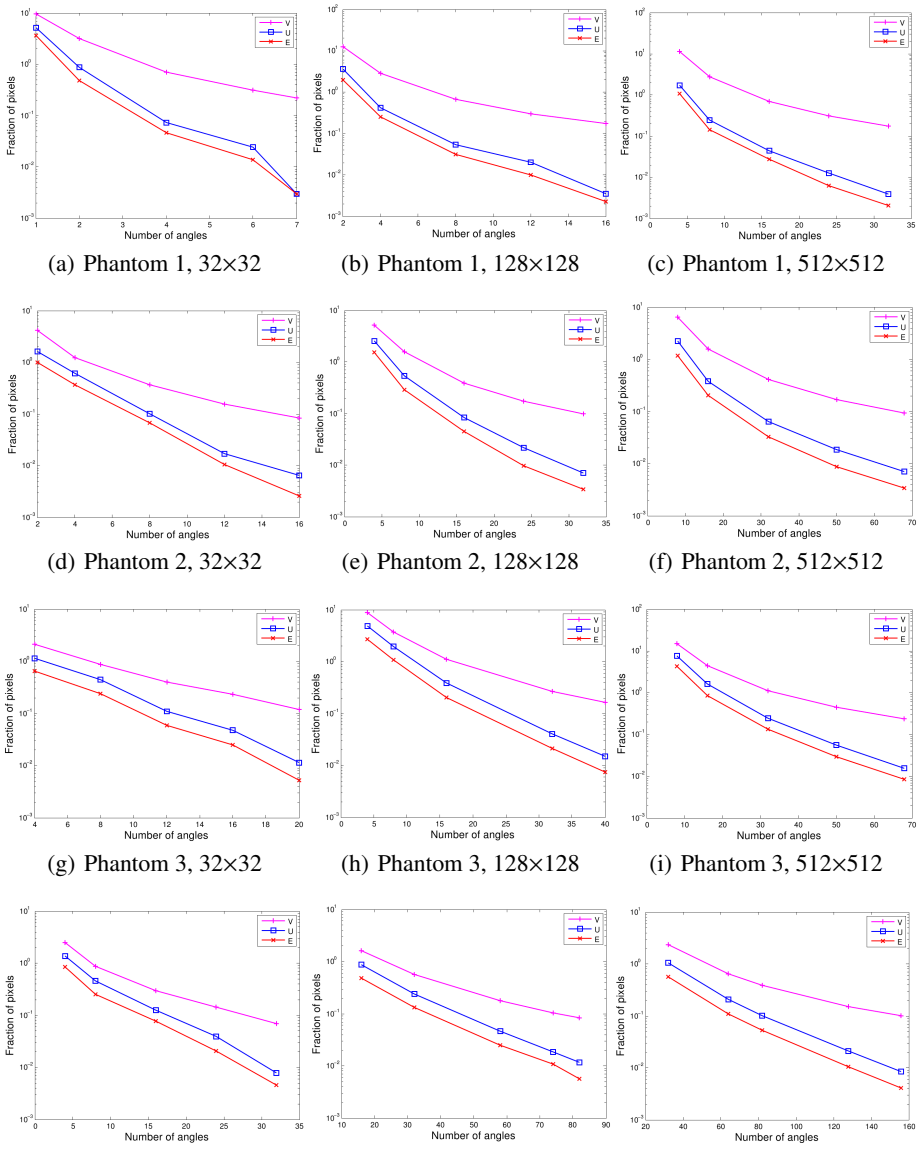

(a) Phantom 1, 32×32 (b) Phantom 1, 128×128 (c) Phantom 1, 512×512

(d) Phantom 2, 32×32 (e) Phantom 2, 128×128 (f) Phantom 2, 512×512

(g) Phantom 3, 32×32 (h) Phantom 3, 128×128 (i) Phantom 3, 512×512

(j) Phantom 4, 32×32 (k) Phantom 4, 128×128 (l) Phantom 4, 512×512

Fig. 3. Grid model: computed bounds as a function of the number of projection directions.

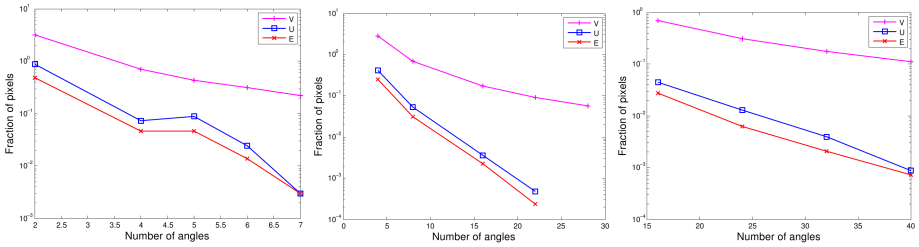

(a) Phantom 1, 32×32 (b) Phantom 1, 128×128 (c) Phantom 1, 512×512

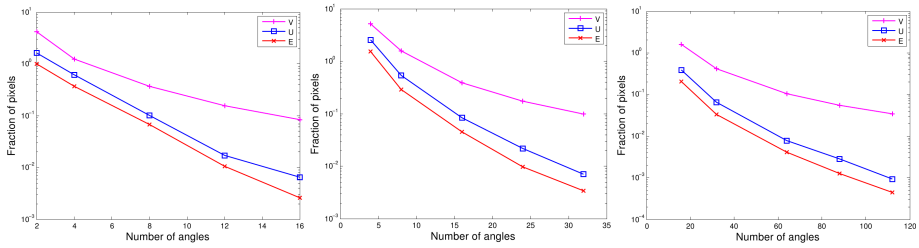

(d) Phantom 2, 32×32 (e) Phantom 2, 128×128 (f) Phantom 2, 512×512

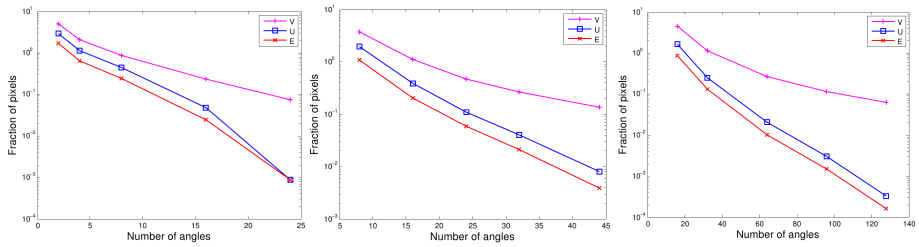

(g) Phantom 3, 32×32 (h) Phantom 3, 128×128 (i) Phantom 3, 512×512

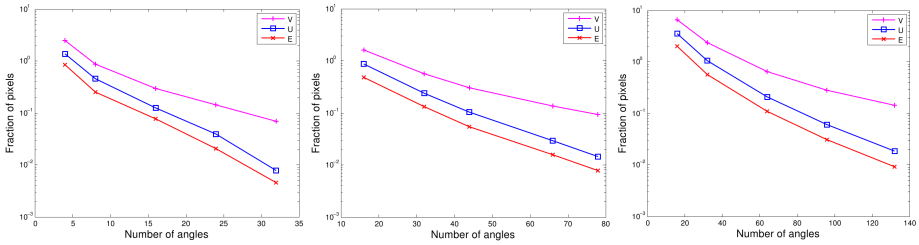

(j) Phantom 4, 32×32 (k) Phantom 4, 128×128 (l) Phantom 4, 512×512

Fig. 4. Strip model: computed bounds as a function of the number of projection directions.

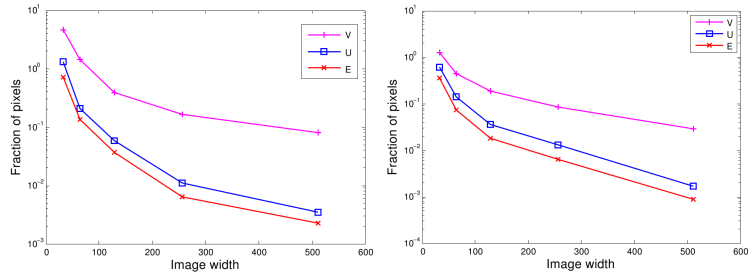

(a) Phantom 1, $\frac{c}{k} = 16$ (b) Phantom 2, $\frac{c}{k} = 8$

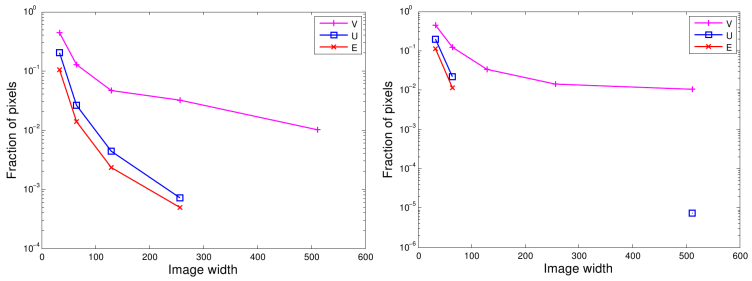

(c) Phantom 3, $\frac{c}{k} = 4$ (d) Phantom 4, $\frac{c}{k} = 4$

Fig. 5. Grid model: computed bounds as a function of the image width c, while keeping the ratio $\frac{c}{k}$ constant.

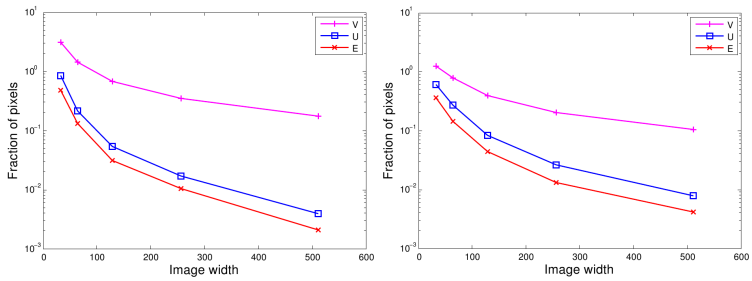

(a) Phantom 1, $\frac{c}{k} = 16$ (b) Phantom 2, $\frac{c}{k} = 8$

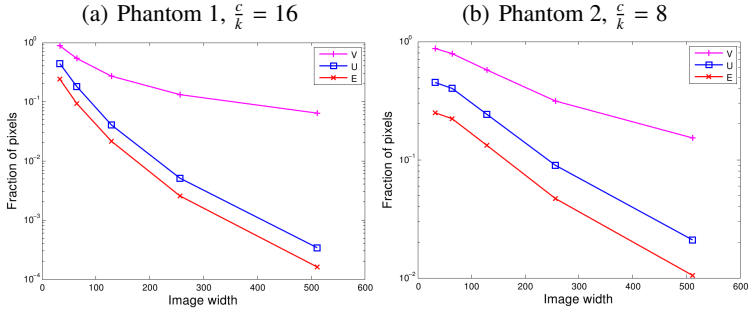

(c) Phantom 3, $\frac{c}{k} = 4$ (d) Phantom 4, $\frac{c}{k} = 4$

Fig. 6. Strip model: computed bounds as a function of the image width c, while keeping the ratio $\frac{c}{k}$ constant.